Postharvest Biology and Technology 143 (2018) 112–118

Contents lists available at ScienceDirect

Postharvest Biology and Technology

journal homepage: www.elsevier.com/locate/postharvbio

SSC and pH for sweet assessment and maturity classification of harvested cherry fruit based on NIR hyperspectral imaging technology

Xiaoli Li[a], Yuzhen Wei[a], Jie Xu[b], Xuping Feng[a], Feiyue Wu[c], Ruiqing Zhou[a], Juanjuan Jin[a], Kaiwen Xu[a], Xinjie Yu[d], Yong He[a,*]

[a] College of Biosystems Engineering and Food Science, Zhejiang University, 866 Yuhangtang Road, Hangzhou 310058, China
[b] College of Biological Chemical Science and Engineering, Jiaxing University, Jiaxing 314001, China
[c] School of Materials and Chemical Engineering, Chongqing University of Arts and Sciences, Chongqing 402160, China
[d] Ningbo Institute of Technology, Zhejiang University, Ningbo 315100, China

ARTICLE INFO

Keywords:
Cherry fruit
SSC
pH
Visualization
Near infrared
Hyperspectral imaging

ABSTRACT

The relationships between soluble solids content (SSC) and pH cherry fruit of different maturity stages has been investigated using near-infrared (NIR) hyperspectral imaging technology. Using 550 fruit, 11 hyperspectral images in the 874–1734 nm region were captured and compared with SSC and pH measured by standard methods. Two types of models based on full bands, namely principal components regression model and partial least squares regression model, showed similar predictive ability. To reduce the modeling complexity based on full bands, a genetic algorithm (GA) and a successive projections algorithm were employed to select feature bands; both algorithms were tested by multiple linear regression (MLR). By comparing the results of different modeling methods, GA-MLR was selected as the final modeling method with a ratio of standard deviation of prediction set to standard deviation of prediction error of 2.7 for SSC and 2.4 for pH. SSC and pH distribution maps were generated by inputting the feature bands of each pixel into GA-MLR models. Classification of fruit maturity stages was studied, and a linear discrimination analysis method produced a correct classification ratio of 96.4%. We conclude that it is feasible to detect the quality of cherry fruit by NIR hyperspectral imaging technology.

1. Introduction

Cherries are a widely consumed fruit that is rich in sugar, vitamins, anthocyanins, minerals and other nutrients (Cao et al., 2015). They have distinct flavors based on cultivar, growing environment and ripening stage (Hayaloglu and Demir, 2015). Cherries can be divided into sour types and the typically consumed sweet type. As with many other fruit, pH and SSC are two important indicators that determine the taste or quality of cherry fruit (Jinping et al., 2015). Both pH and SSC measurements require destructive sampling, and also are not suitable for on-line detection.

The characteristics and substance of fruit can be reflected in spectra and many applications have been described, such for apple, kiwifruit, mango and pear quality detection (Fan et al., 2009; Li et al., 2013; Moghimi et al., 2010; Neto et al., 2017). Spectral studies on cherries include Vis-NIR measurement of SSC using PLS regression (Carlini et al., 2000), and a cherry meter for ripening and quality assessment (Nagpala et al., 2017). All of these studies depend solely on spectral information, but only applying spectroscopic techniques to determine the fruit substance may not be adequate in some cases, because it is difficult to measure multiple samples simultaneously, and there is no visualization.

Hyperspectral images contain both spectral and image information (Manley, 2014), can fulfill the task of visualization (Gowen et al., 2007), and improve the efficiency of detection. As a result, hyperspectral imaging technology has been applied to many fields (Feng and Sun, 2012), including food (Zhang et al., 2014) and agricultural industries (He and Sun, 2015). Studies include quality and safety assessment of fruit and vegetables, detection of pits in tart cherries (Qin and Lu, 2004), jujube defects (Wu et al., 2016), and cracking (Yu et al., 2014), as well as lime quality and maturity index grading (Teerachaichayut and Ho, 2017), sugariness and hardness distribution visualization of melons (Sun et al., 2016) and blueberries (Leivavalenzuela et al., 2013), and visualization of fiber content in celeries (Ling et al., 2017). Furthermore, hyperspectral imaging technology can be used in the quality inspection of meats and grains,

* Corresponding author.
E-mail address: yhe@zju.edu.cn (Y. He).

https://doi.org/10.1016/j.postharvbio.2018.05.003
Received 25 September 2017; Received in revised form 8 May 2018; Accepted 8 May 2018
Available online 13 May 2018
0925-5214/

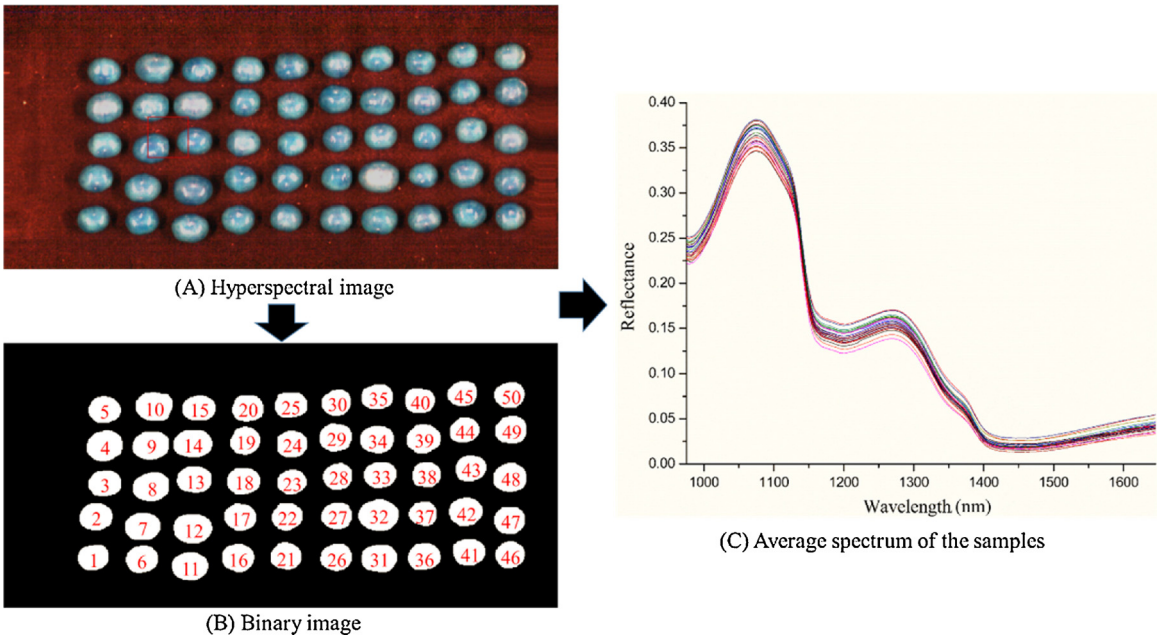

Fig. 1. (A) Hyperspectral image in pseudo color, the RGB channels corresponded to 1399 nm, 1197 nm and 995 nm, respectively; (B) Binary image of cherry fruit region; (C) Spectra of all samples, each spectrum was obtained by calculating the average of all the pixels belonging to the same sample.

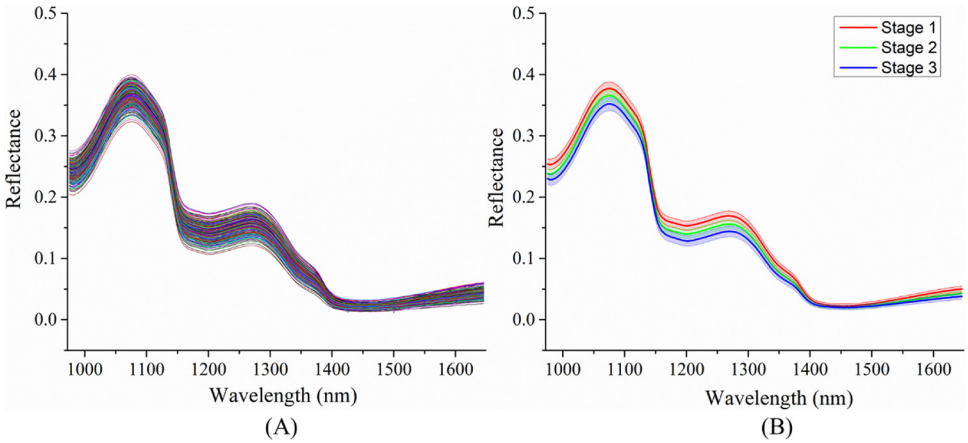

Fig. 2. (A) Spectral curves of all samples; (B) Average ± SD of three maturity stages, it meant average spectrum plus or minus standard deviation of all samples which belong to the same maturity stage. The average spectrum was represented by the line with dark color. The positive and negative standard deviation were represented by the upper and lower boundaries of the area with light translucent color.

reports about pH and tenderness visualization of beef (Elmasry et al., 2012), chemical spoilage extent traceability of processed pork (Cheng et al., 2017) and fusarium damage visualization in wheat kernels (Delwiche et al., 2011). However, no research on cherry flavor detection or maturity stage classification based on near-infrared hyperspectral imaging has been reported.

NIR spectroscopy is mainly generated from double and combination frequency absorption of molecular vibration as well as Fermi resonance. It is very suitable for the measurement of organic matter with hydrogen groups (Cen and He, 2007), which includes soluble sugar and organic acids such as glucose, fructose, malic acid and citric acid.

The objectives of this study were to investigate the use of NIR hyperspectral imaging technology on cherry fruit to 1) Establish regression models for SSC and pH, 2) Simultaneously detect multiple individuals in a visual manner, and 3) Classify maturity stages.

2. Material and methods

2.1. Sample preparation

'Hongdeng' cherry fruit of good condition without lesions or bruises were harvested on May 26, 2017 in Tingkou Town, Qixia District, Yantai City, Shandong Province, China. A total of 550 fruit were divided by 5 orchardists to provide 200 fruit in each of maturity stages 1 and 3, and 150 fruit of maturity stage 2. As a single cherry fruit has too little juice, two cherry fruit were treated as one sample to squeeze juice for measurement. The juice was collected into a 10 mL centrifuge tube. The SSC values were obtained through dropping 1 mL juice into the test slot of a portable refractive index instrument (30 GS, Mettler-Toledo Company, Switzerland), and the pH values were determined through inserting the probe of a pH instrument (AZ 8601, Hengxin Company, China) into the juice. After chemical indicator measurement, 275 samples were obtained for further analysis.

2.2. Sample division method

Reasonable sample division is essential to establish a robust model. An ideal sample division method should meet the following basic conditions: 1) The concentration fluctuation range of the calibration set should exceed the range of the prediction set. 2) The calibration set should have enough samples to determine the mathematical relationship between spectral variables and concentrations. 3) The concentration values of the calibration set should be distributed evenly.

The interval sampling (IS) method was adopted to satisfy the above

Table 1
Statistical results of the calibration set and prediction set SSC and pH.

Index	Set	Number of samples	Maximum	Minimum	Average	SD
SSC	Calibration	220	21.3	8.6	13.82	3.286
	Prediction	55	20.3	8.8	13.822	3.295
	Total	275	21.3	8.6	13.82	3.282
pH	Calibration	220	4.1	3.3	3.639	0.138
	Prediction	55	4	3.4	3.64	0.136
	Total	275	4.1	3.3	3.639	0.137

Table 2
SSC and pH (mean ± SD) of fruit at different maturity stages.

Maturity Stage	SSC	pH
1	10.53 ± 1.35c	3.52 ± 0.1c
2	13.23 ± 0.82b	3.64 ± 0.07b
3	17.55 ± 1.5a	3.76 ± 0.1a

Table 3
Performance of PCR and PLSR models for SSC and pH.

Substance	Model	PCs or LVs	R_C^2	RMSEC	R_P^2	RMSEP	RPD
SSC	PCR	37	0.867	1.197	0.836	1.324	2.467
	PLSR	17	0.882	1.125	0.833	1.336	2.444
PH	PCR	5	0.806	0.060	0.805	0.060	2.263
	PLSR	6	0.813	0.059	0.804	0.060	2.258

Table 4
Performance of MLR models of SSC and pH based on different feature band selection methods.

Substance	Method	Bands Num.	R_C^2	RMSEC	R_P^2	RMSEP	RPD
SSC	SPA	28	0.854	1.254	0.771	1.563	2.089
	GA	54	0.897	1.054	0.863	1.210	2.700
PH	SPA	28	0.832	0.056	0.815	0.057	2.326
	GA	24	0.824	0.057	0.819	0.057	2.351

conditions and obtain an ideal calibration set in this study. First, samples were sorted in ascending or descending order according to their chemical concentration values. After sorting, each of five consecutive samples was regarded as a subset, and in each subset, the middle sample was selected to form the prediction set, and the remaining samples were used to form the calibration set.

2.3. Hyperspectral imaging system

The hyperspectral imaging system mainly consists of a camera obscura, a spectrometer (N17E-QE, Specim spectral Imaging Oy Ltd, Finland), lens (OLE-23, Specim spectral Imaging Oy Ltd, Finland), a linear light source (Fiber-Lite DC 950, Dolan Jenner Industries Co., USA), a computer and a mobile platform. The image size of the system is 320 pixels × 256 pixels, the spectral range is 874–1734 nm, and the spectral resolution is 5 nm.

During the experiment, the mobile platform movement speed was set to 22.5 mm s^{-1}, the camera exposure time was set to 3 ms, and the distance between the lens and the samples was set to 30.5 cm.

2.4. Spectral data acquisition

To eliminate the impacts of uneven illumination and dark current noise, the raw hyperspectral image was calibrated by standard white and dark reference images according to the following formula

$$R_c = \frac{R_0 - B}{W - B}$$

where R_o indicates the raw hyperspectral image, R_c means the calibrated hyperspectral image, W represents the standard white reference image obtained by using a rectangular Teflon plate, and B denotes the standard black reference image obtained by covering the lens completely with an opaque black cover.

The process of the spectral data acquisition is shown in Fig. 1. Fig. 1A shows the captured hyperspectral image in pseudo color. The spectral characteristics of cherry fruit and background were analyzed with ENVI 4.8 software (Boulder, USA), then a proper reflectivity threshold of 0.15 at the 1106 nm band was identified to separate cherry fruit from background. After separation, every fruit region was marked in the binary image as shown in Fig. 1B; the serial numbers were tagged in order from bottom to top and left to right. Two fruit of adjacent single and double numbers were taken as one sample, such as '1′ and '2′, '3′ and '4′. According to the serial numbers, average spectrum of every sample was calculated with Matlab 2017a software (Mathworks, USA), and the spectra of all the samples in the image was obtained (Fig. 1C).

2.5. Feature band selection

Each pixel in the hyperspectral image consists of 256 variables, and a collinearity problem always exists among these variables, which will cause information redundancy and increase the amount of modeling calculations. Therefore, feature band selection is necessary to reduce the calculation demands and improve the stability of the models.

Genetic algorithm (GA) and successive projections algorithm (SPA)

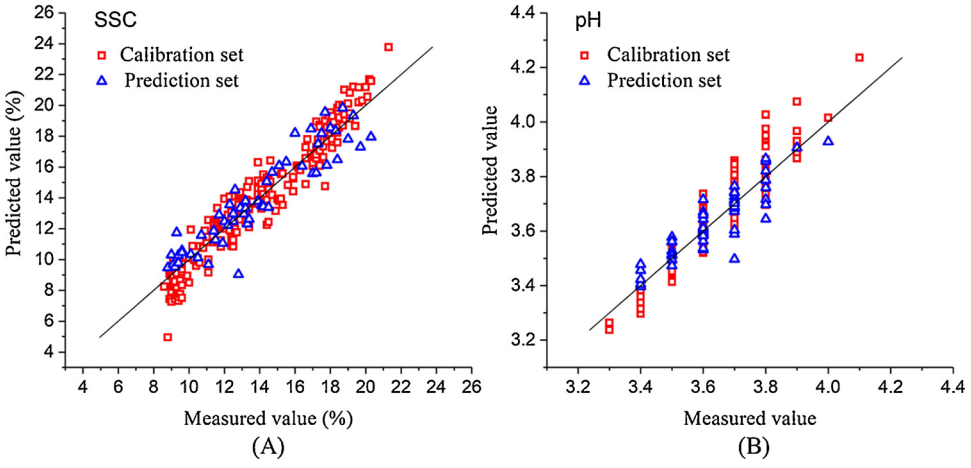

Fig. 3. The scatter plot of measured versus predicted values of SSC (A) and pH (B) for the calibration set and the prediction set. The red rectangles and blue triangles represent the samples of the calibration set and the prediction set, respectively, the abscissa values and ordinate values of rectangles or triangles represent the concentration values measured by instruments and predicted by models, respectively, and the slash in each coordinate represents the standard line (For interpretation of the references to colour in this figure legend, the reader is referred to the web version of this article.).

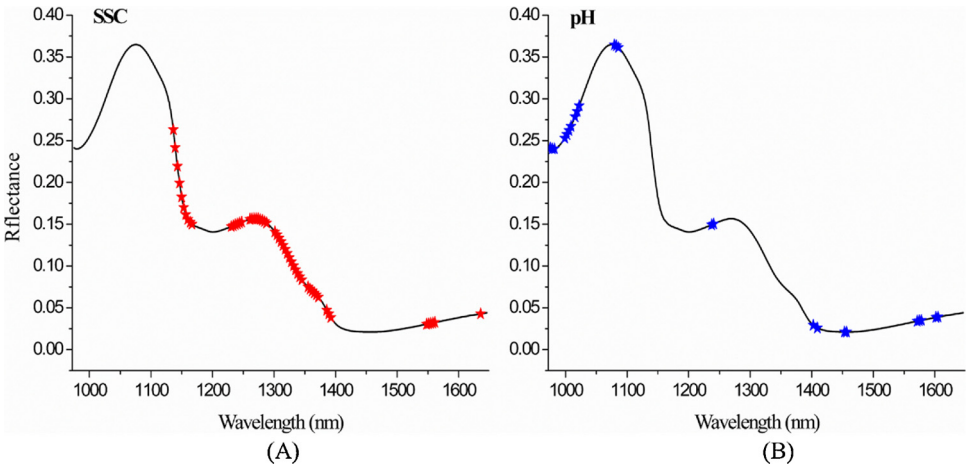

Fig. 4. The distribution of characteristic bands of SSC (A) and pH (B) in the spectral curve. In this figure, each pentagram marks the position of a feature band in the spectral curve.

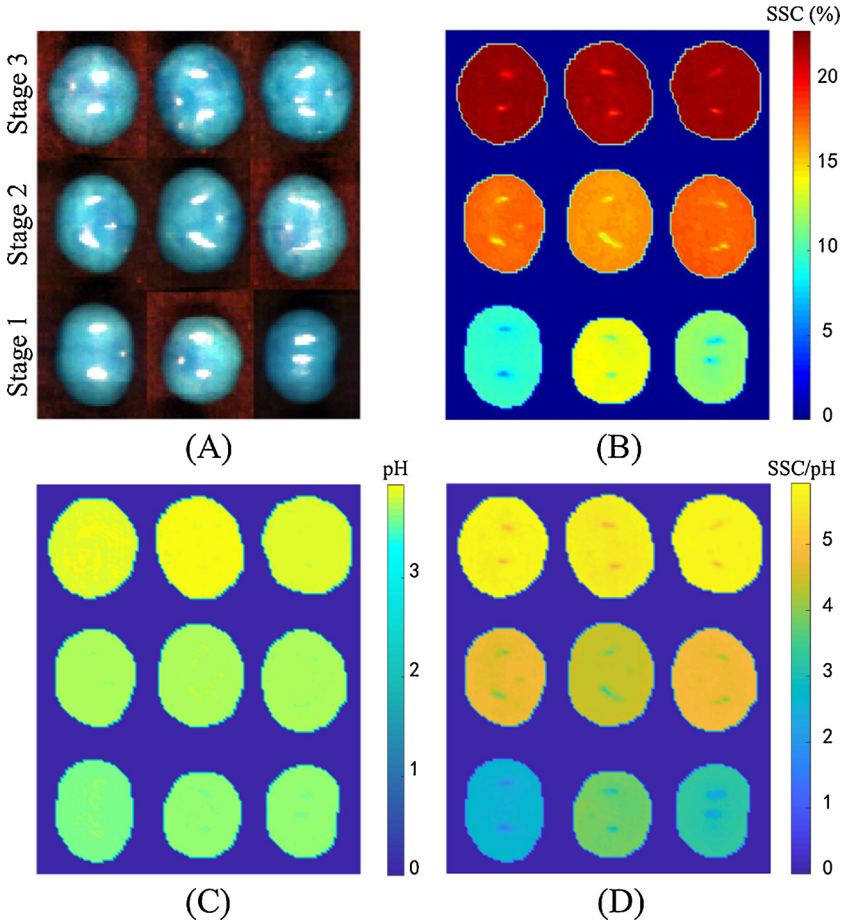

Fig. 5. (A) Original RGB graph captured by the NIR-HSI system. In this graph, cherry fruit in the same row have the same maturity stage, and the maturity stages are marked on the left of graph; (B) Distribution map of SSC; (C) Distribution map of pH; (D) Distribution map of SSC/pH.

are variable selection methods that were used. GA is a computational model that simulates natural selection of biological evolution theory and biological evolution processes of genetic mechanisms. It is a stochastic or random search method to find the optimal solution by simulating the natural evolution processes (Ying and Liu, 2008), which mainly consists of the following five steps: (1) variable coding; (2) population initiation; (3) response evaluation; (4) reproduction; and (5) mutation. After finishing step 5 the first time, the loops of step 3–5 will be executed until the criterion is satisfied. SPA provides a direct method to solve the collinearity problem (Li et al., 2015); the method starts at one wavelength and calculates its projection at the unselected wavelength in each loop. The wavelength with the maximum projection vector is introduced into the wavelength combination (Araújo et al., 2001).

2.6. Model building and evaluation

Two typical methods, principal components regression (PCR) and

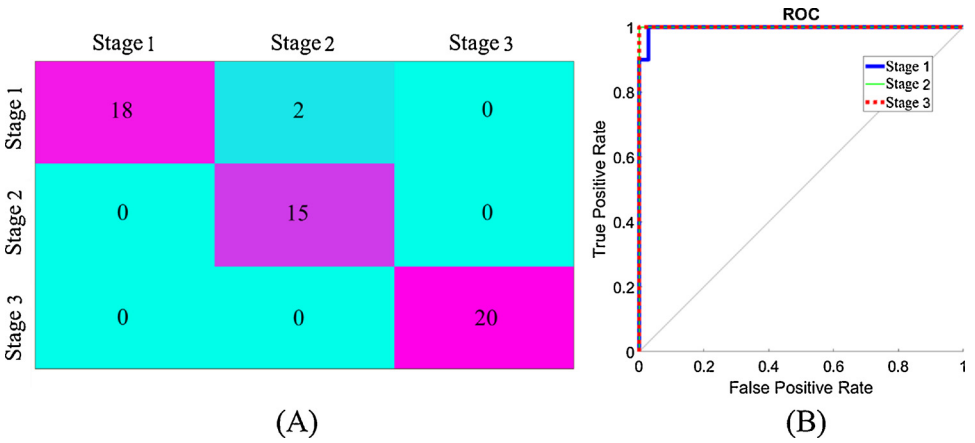

Fig. 6. (A) Confusion matrix, the stages marked on the left are the actual, original categories, and the stages marked on the top are the categories obtained by the classifiers. The sums of numbers on the diagonal line are the correct classification number, and the sums of numbers in other positions are the misclassification numbers; (B) ROC, the coordinate in each position of the curve consists of the true positive rate and false positive rate under a certain threshold, and the diagonal line is the reference line generated by random guess.

partial least square regression (PLSR), were applied to establish models between full bands and chemical concentration, respectively. The basic principle of PCR is to recombine the original variables with a certain correlation into uncorrelated variables as principal components (Sun, 1995), then the regression model based on the principal components is established. PLSR is similar to PCR, the difference being that PCR extract principal components only on the basis of independent variables while PLSR makes a comprehensive consideration of independent and dependent variables (Helland and Inge, 2006). Multiple linear regression (MLR) was employed to build models between feature bands and chemical concentration. MLR is a simple and typical regression method, which calculates the coefficients of each independent variable based on the principle of minimizing the prediction error (Andrews, 1974). The linear discriminant analysis (LDA) method was utilized to build the classification model for cherry maturity stages. LDA takes the strategy to classify categories through projecting the variables to the best discriminant vector space (Ye, 2007).

After establishment of the regression model, the root mean square error of calibration and prediction (RMSEC and RMSEP), the determination coefficient of calibration and prediction (R_C^2 and R_P^2) and standard deviation of prediction set to standard deviation of prediction error (RPD) were employed to evaluate the performance of the regression models. For evaluation of classification results, a confusion matrix and receiver operating characteristic (ROC) curve were used to describe the performance.

2.7. Visualization of concentration distribution

As the shape of cherry fruit is approximately spherical, spectra of different pixels in the same fruit region may vary tremendously. This issue will worsen the imaging results. Through calibrating the spectra with depth information (Karaca et al., 2014; Rueda et al., 2017; Zia et al., 2015) or prior knowledge (Gómez-Sanchis et al., 2008; Zhang et al., 2015), the adverse effect caused by the shape can be reduced significantly. However, these methods increase the cost and complexity of system, reducing stability and real-time performance of practical applications.

In the light of the specific application of cherry fruit detection, the fundamental purpose is to detect the holistic quality of a fruit, like average pH and SSC. The expression of local features of a cherry fruit is secondary. Based on this fact, an effective scheme was proposed to calibrate the spectra. In this scheme, average spectrum of a fruit was calculated, and the deviation of all pixels belonging to the same fruit were compressed to a reasonable range. The deviation range was compressed to 1/3 that of the calibration set, supposing that the deviations of three maturity levels are equal. In fact, the deviations can be compressed to a smaller range.

The average spectrum plus the compressed deviation was taken as the final input variable for each pixel. As the average spectrum and the processed deviation can reflect the global and local characteristics respectively, through importing the final input variables into the regression model, reasonable concentration values can be obtained for all pixels, and the distribution of SSC and pH in cherry fruit will be displayed visually.

3. Results and discussion

3.1. Spectral characteristics

As there is obvious noise in the front and rear regions of the spectrum, 200 bands in the 972-1649-nm region were selected as effective bands. Spectral curves in the effective region of all samples are shown in Fig. 2A. All the spectral curves have similar trends, but they are dissimilar in reflectance intensity, which indicates that different fruit basically have the same internal substance, but the individual compounds are different in content. The difference in spectral reflectance intensity provides a premise for establishing the regression model.

Average spectral curves with a deviation of three maturity stages are shown in Fig. 2B. It is easy to distinguish different maturity stages due to distinct average and deviations, especially for maturity stages 1 and 3. Therefore, there is convincing evidence to support the feasibility of maturity stage classification through spectral information.

3.2. Statistical analysis of chemical concentration values

All samples were divided into a calibration set and a prediction set according to the IS method mentioned in Section 2.2, a calibration set with 220 samples and a prediction set with 55 samples were obtained. The statistical characteristics of SSC and pH in the calibration set and the prediction set are shown in Table 1.

The sample size of the calibration set is four times that of the prediction set for both SSC and pH (Table 1) and the concentration fluctuation amplitude of the calibration set is greater than that of the prediction set. The SDs of the calibration set, the prediction set and all the samples are close. Therefore, the IS method is appropriate for sample division, according to the conditions mentioned in Section 2.2.

The statistical characteristics of SSC and pH at the three maturity stages were also analyzed, and the results are shown in Table 2.

Differences between averages at $P = 1.52e^{-111}$ and $1.29e^{-46}$ (for SSC and pH respectively) are indicated by lowercase letters. The data illustrate that maturity stage is strongly correlated with SSC and pH of the cherry fruit.

3.3. Modeling based on full bands

After all samples were divided into the calibration set and the

prediction set, PCR and PLSR models based on full bands were built. The performance of models for SSC were better than the models for pH (Table 3), perhaps because of the characteristics of pH value distribution. The fluctuation range of pH values is small, and the pH values only range from 3.3 to 4.1 with an interval of 0.1.

For both SSC and pH, the prediction accuracy of PCR is slightly better than that of PLSR (Table 3). But it is difficult to determine which modeling method has better performance, as only one case of sample division may bring randomness. There was no significant difference between PCR and PLSR ($P = 0.913$) through analysis of variance for five cases of sample division. In the light of data compression process, PCR extracted principal components only according to the spectral matrix, while principal components of PLSR were extracted based on the spectral matrix and the concentration matrix synthetically (Ergon, 2013). A good linear relationship between the spectral data and the concentration data was found since there was no effect of considering concentration data.

3.4. Modeling based on feature bands

GA appears superior to SPA through the set proper parameters (Table 4), so GA was applied to extract the feature bands to establish the MLR model. Fifty four bands were selected for the SSC model, and 24 bands were selected for the pH model. The performance of the SSC and pH models based on feature bands was slightly improved compared with that of the models using full bands, and all five model evaluation parameters improved to some extent. Fig. 3A and B show the modeling and prediction performance for SSC and pH.

By comparing Fig. 4A and B, obvious differences in feature band distribution were easily found in the three regions. The first region is 972–1100 nm, and this region contains feature bands of pH but does not contain feature bands of SSC, while in the second region (1100-1200 nm) and the third region (1250-1350 nm), the opposite is true. The specific characteristics of the first region may result from vibrations of hydrogen groups, such as O—H and N—H, and acidic compounds usually contain hydrogen groups; however, absorbance peaks in the second and third regions are mainly caused by C═O (1160 nm) and C—H (1170 nm, 1194 nm) vibration (Burns and Ciurczak, 2008), and these two chemical bonds are ubiquitous in soluble sugar, which is a major component of SSC.

3.5. Visualization of concentration distribution

Three fruit belonging to each maturity stage were selected to generate distribution maps of SSC and pH (Fig. 5). Before generating distribution maps, the feature bands of each pixel of fruit were calibrated according to the method mentioned in Section 2.7 as the final input variables. Importing the variables into GA-MLR models, differences in SSC and pH between different fruit can be observed (Fig. 5B and C). Because flavor is affected determined by both SSC and pH (reference required), a pseudo-color map of SSC/pH was generated (Fig. 5D). Combining distribution maps of SSC, pH and SSC/pH would be useful for monitoring the quality of cherry fruit on-line.

3.6. Maturity stage classification

The LDA model was designed to classify cherry maturity stages. Through the confusion matrix (Fig. 6A), the total accuracy of correct classification is 96.4%, and only two samples originally belonging to stage 1 were wrongly identified as stage 2. Through the receiver operator characteristic (ROC) curve in Fig. 6B, the classifier for the three maturity stages is relatively precise as the areas under the curve are all greater than 0.95.

To ensure consistency, classification of each maturity stage was performed by five orchardists based on the principle of obedience to the majority while the judgements of orchardists are inconsistent in this research. But in actual production, the maturity stage is usually judged by only one orchardist, this will cause a problem of uniformity as the criterions of different orchardists are not exactly consistent. Therefore, it is necessary to develop a stable and objective classification method to replace artificial methods. The LDA method shows excellent performance, it can serve as a reference as its criterion for judgement was integrated with the experience of multiple orchardists.

4. Conclusion

NIR hyperspectral imaging technology was adopted for visual detection of cherry fruit quality and classification of maturity stages. In general, the results are satisfactory based on the concentration distribution maps, SSC and pH of the cherries, and the classification of three maturity stages was shown to be feasible with high accuracy. This research provides a scheme to simultaneously detect multiple fruit online, which makes it suitable for actual production. In future work, more samples with different cultivars and growing places will be collected to improve the universality of the model, as the difference in SSC and pH between different cultivars and grow places are more obvious.

Acknowledgments

This research was funded by the National Natural Science Foundation of China (No: 31771676), the Technological Research Program of the Chongqing Municipal Education Commission (Project No: KJ1501128), the Zhejiang Province Public Technology Research Program (Project No: 2015C02008) and (Project No: 2017C02027), the Zhejiang Province Public Welfare Technology Application Research Project (Project No: 2014C32091), and the Special Funding Projects for Basic Scientific Research Projects in Universities (Project No: 2015QNA6005).

References

Andrews, D.F., 1974. A robust method for multiple linear regression. Technometrics 16 (4), 523–531. http://dx.doi.org/10.2307/1267603.

Araújo, M.C.U., Saldanha, T.C.B., Galvão, R.K.H., Yoneyama, T., Chame, H.C., Visani, V., 2001. The successive projections algorithm for variable selection in spectroscopic multicomponent analysis. Chemom. Intell. Lab. Syst. 57 (2), 65–73. http://dx.doi.org/10.1016/s0169-7439(01)00119-8.

Burns, D.A., Ciurczak, E.W., 2008. Handbook of Near-Infrared Analysis, third ed. CRC Press, Boca Raton, pp. 431–433. http://dx.doi.org/10.1201/9781420007374.

Cao, J., Li, X., Liu, Y., Leng, F., Li, X., Sun, C., Chen, K., 2015. Bioassay-based isolation and identification of phenolics from sweet cherry that promote active glucose consumption by HepG2 cells. J. Food Sci. 80 (2), 234–240. http://dx.doi.org/10.1111/1750-3841.12743.

Carlini, P., Massantini, R., Mencarelli, F., 2000. Vis-NIR measurement of soluble solids in cherry and apricot by PLS regression and wavelength selection. J. Agric. Food Chem. 48 (11), 5236–5242. http://dx.doi.org/10.1021/jf000408f.

Cen, H., He, Y., 2007. Theory and application of near infrared reflectance spectroscopy in determination of food quality. Trends Food Sci. Tech. 18 (2), 72–83. http://dx.doi.org/10.1016/j.tifs.2006.09.003.

Cheng, W., Sun, D.W., Pu, H., Wei, Q., 2017. Chemical spoilage extent traceability of two kinds of processed pork meats using one multispectral system developed by hyperspectral imaging combined with effective variable selection methods. Food Chem. 221, 1989–1996. http://dx.doi.org/10.1016/j.foodchem.2016.11.093.

Delwiche, S.R., Kim, M.S., Dong, Y., 2011. Fusarium damage assessment in wheat kernels by Vis/NIR hyperspectral imaging. Sens. Instrum. Food Qual. Saf. 5 (2), 63–71. http://dx.doi.org/10.1007/s11694-011-9112-x.

Elmasry, G., Sun, D.W., Allen, P., 2012. Near-infrared hyperspectral imaging for predicting colour, pH and tenderness of fresh beef. J. Food Eng. 110 (1), 127–140. http://dx.doi.org/10.1016/j.jfoodeng.2011.11.028.

Ergon, R., 2013. Principal Component Regression (PCR) and Partial Least Squares Regression (PLSR). John Wiley & Sons, Ltd, Hoboken, pp. 121–142. http://dx.doi.org/10.1002/9781118434635. ch08.

Fan, G., Zha, J., Du, R., Gao, L., 2009. Determination of soluble solids and firmness of apples by Vis/NIR transmittance. J. Food Eng. 93 (4), 416–420. http://dx.doi.org/10.1016/j.jfoodeng.2009.02.006.

Feng, Y.Z., Sun, D.W., 2012. Application of hyperspectral imaging in food safety inspection and control: a review. Crit. Rev. Food Sci. Nutr. 52 (11), 1039–1058. http://dx.doi.org/10.1080/10408398.2011.651542.

Gómez-Sanchis, J., Moltó, E., Camps-Valls, G., Gómez-Chova, L., Aleixos, N., Blasco, J., 2008. Automatic correction of the effects of the light source on spherical objects. An application to the analysis of hyperspectral images of citrus fruits. J. Food Eng. 85

(2), 191–200. http://dx.doi.org/10.1016/j.jfoodeng.2007.06.036.
Gowen, A.A., O'Donnell, C.P., Cullen, P.J., Downey, G., Frias, J.M., 2007. Hyperspectral imaging – an emerging process analytical tool for food quality and safety control. Trends Food Sci. Tech. 18 (2), 590–598. http://dx.doi.org/10.1016/j.tifs.2007.06.001.
Hayaloglu, A.A., Demir, N., 2015. Physicochemical characteristics, antioxidant activity, organic acid and sugar contents of 12 sweet cherry (*Prunus avium* L.) cultivars grown in Turkey. J. Food Sci. 80 (3), 564–570. http://dx.doi.org/10.1111/1750-3841.12781.
He, H.J., Sun, D.W., 2015. Hyperspectral imaging technology for rapid detection of various microbial contaminants in agricultural and food products. Trends Food Sci. Tech. 46 (1), 99–109. http://dx.doi.org/10.1016/j.tifs.2015.08.001.
Helland, Inge, 2006. Partial Least Squares Regression. John Wiley & Sons, Ltd, Hoboken, pp. 97–114. http://dx.doi.org/10.1002/0471667196.ess6004.pub2.
Jinping, C., Qing, J., Juanying, L., Xian, L., Chongde, S., Kunsong, C., 2015. Physicochemical characterisation of four cherry species (Prunus spp.) grown in China. Food Chem. 173, 855–863. http://dx.doi.org/10.1016/j.foodchem.2014.10.094.
Karaca, A.C., Çeşmeci, D., Ertürk, A., Güllü, M.K., Ertürk, S., 2014. Hyperspectral change detection with stereo disparity information enhancement. IEEE Workshop on Hyperspectral Image and Signal Processing: Evolution in Remote Sensing. http://dx.doi.org/10.1109/whispers.2014.8077541.
Leivavalenzuela, G.A., Lu, R., Aguilera, J.M., 2013. Prediction of firmness and soluble solids content of blueberries using hyperspectral reflectance imaging. J. Food Eng. 115 (1), 91–98. http://dx.doi.org/10.1016/j.jfoodeng.2012.10.001.
Li, J., Huang, W., Zhao, C., Zhang, B., 2013. A comparative study for the quantitative determination of soluble solids content, pH and firmness of pears by Vis/NIR spectroscopy. J. Food Eng. 116 (2), 324–332. http://dx.doi.org/10.1016/j.jfoodeng.2012.11.007.
Li, X., Sun, C., Zhou, B., He, Y., 2015. Determination of hemicellulose, cellulose and lignin in moso bamboo by near infrared spectroscopy. Sci. Rep. 5http://dx.doi.org/10.1038/srep17210. Paper Number: 17210.
Ling, Y., Xiong, C., Hao, Q., Liu, C., Wei, C., Lei, Z., 2017. Non-destructive determination and visualisation of insoluble and soluble dietary fibre contents in fresh-cut celeries during storage periods using hyperspectral imaging technique. Food Chem. 228, 249–256. http://dx.doi.org/10.1016/j.foodchem.2017.02.010.
Manley, M., 2014. Near-infrared spectroscopy and hyperspectral imaging: non-destructive analysis of biological materials. Chem. Soc. Rev. 43 (24), 8200–8214. http://dx.doi.org/10.1117/12.2262862.5460497462001.
Moghimi, A., Aghkhani, M.H., Sazgarnia, A., Sarmad, M., 2010. Vis/NIR spectroscopy and chemometrics for the prediction of soluble solids content and acidity (pH) of kiwifruit. Biosyst. Eng. 106 (3), 295–302. http://dx.doi.org/10.1016/j.biosystemseng.2010.04.002.
Nagpala, E.G.L., Noferini, M., Farneti, B., Piccinini, L., Costa, G., 2017. Cherry-Meter: an innovative non-destructive (vis/NIR) device for cherry fruit ripening and quality assessment. Acta Hortic. 1161, 491–496. http://dx.doi.org/10.17660/actahortic.2017.1161.78.
Neto, J.P.D.S., Assis, M.W.D.D., Casagrande, I.P., Júnior, L.C.C., 2017. Determination of 'Palmer' mango maturity indices using portable near infrared (VIS-NIR) spectrometer. Postharv. Biol. Technol. 130, 75–80. http://dx.doi.org/10.1016/j.postharvbio.2017.03.009.
Qin, J., Lu, R., 2004. Detecting pits in tart cherries by hyperspectral transmission imaging. Proc. SPIE. 48 (5), 1963–1970. http://dx.doi.org/10.13031/2013.19988.
Rueda, H., Chen, F., Lau, D.L., Arce, G.R., 2017. Single aperture spectral + ToF compressive camera: toward hyperspectral + depth imagery. IEEE J-STSP. 11 (7), 992–1003. http://dx.doi.org/10.1109/jstsp.2017.2737784.
Sun, J.G., 1995. A correlation principal component regression-analysis of NIR data. J. Chemom. 9 (1), 21–29. http://dx.doi.org/10.1002/cem.1180090104.
Sun, M., Zhang, D., Liu, L., Wang, Z., 2016. How to predict the sugariness and hardness of melons: a near-infrared hyperspectral imaging method. Food Chem. 218, 413–421. http://dx.doi.org/10.1016/j.foodchem.2016.09.023.
Teerachaichayut, S., Ho, H.T., 2017. Non-destructive prediction of total soluble solids, titratable acidity and maturity index of limes by near infrared hyperspectral imaging. Postharv. Biol. Technol. 133, 20–25. http://dx.doi.org/10.1016/j.postharvbio.2017.07.005.
Wu, L., He, J., Liu, G., Wang, S., He, X., 2016. Detection of common defects on jujube using Vis-NIR and NIR hyperspectral imaging. Postharvest Biol. Technol. 112, 134–142. http://dx.doi.org/10.1016/j.postharvbio.2015.09.003.
Ye, J., 2007. Least squares linear discriminant analysis. Machine Learning, Proceedings of the Twenty-Fourth International Conference 3 (10), 1087–1093. http://dx.doi.org/10.1145/1273496.1273633.
Ying, Y., Liu, Y., 2008. Nondestructive measurement of internal quality in pear using genetic algorithms and FT-NIR spectroscopy. J. Food Eng. 84 (2), 206–213. http://dx.doi.org/10.1016/j.jfoodeng.2007.05.012.
Yu, K., Zhao, Y., Li, X., Shao, Y., Zhu, F., He, Y., 2014. Identification of crack features in fresh jujube using Vis/NIR hyperspectral imaging combined with image processing. Comput. Electron. Agr. 103, 1–10. http://dx.doi.org/10.1016/j.compag.2014.01.016.
Zhang, B., Huang, W., Li, J., Zhao, C., Fan, S., Wu, J., Liu, C., 2014. Principles, developments and applications of computer vision for external quality inspection of fruits and vegetables: a review. Food Res. Int. 62, 326–343. http://dx.doi.org/10.1016/j.foodres.2014.03.012.
Zhang, B., Li, J., Huang, W., Wang, C., Zhao, C., Liu, C., Huang, D., 2015. A study on spectral analysis combining with image processing for lightness correction in spherical fruits by using hyperspectral imaging. 2015 ASABE Annual International Meeting. http://dx.doi.org/10.13031/aim.20152189660. Paper Number: 152189660.
Zia, A., Zhou, J., Gao, Y., 2015. Relative depth estimation from hyperspectral data. 2015 International Conference on Digital Image Computing: Techniques and Applications (DICTA) 1–7. http://dx.doi.org/10.1109/dicta.2015.7371299.